An Active CM and DM EMI Filter Based on Synthesized and Synchronized Signals for the DC Input of a GaN Inverter

Andreas Bendicks, Sebastian Windhövel, Michael Gerten, Stephan Frei

On-board Systems Lab, TU Dortmund University, Dortmund, Germany

Corresponding author: Andreas Bendicks, andreas.bendicks@tu-dortmund.de

Abstract

In this contribution, the electromagnetic common- and differential-mode emissions at the input of a GaN-based inverter are actively suppressed by a cancellation system that synchronously injects two artificially synthesized cancellation signals. Due to the periodic operation, the synthesis can be done from a set of sine waves that can be adjusted very precisely in amplitude and phase. The mutual coupling between the injectors is respected and counterbalanced during signal synthesis. Suitable injecting and decoupling circuits are selected and dimensioned for the system. Measurement results show the very high performance of the proposed method for frequencies of up to 30 MHz.

1   Introduction

Power electronic systems tend to be considerable sources of e**l**ectro**m**agnetic **i**nterferences (EMI) due to the frequently switching power transistors. To comply with international standards on **e**lectro**m**agnetic **c**ompatibility (EMC), e.g. CISPR 25 for automobiles [1], the conducted EMI is commonly reduced by applying passive filters that are often bulky and heavy [2]. To resolve this issue, active cancellation techniques can be applied that aim at a destructive interference between noise and anti-noise [3].

In EMC, **a**ctive **E**MI **f**ilters (AEFs) have been developed in, e.g., [4]-[7] and further analyzed and systemized in, e.g., [8] and [9]. Like passive EMI filters, AEFs are connected between the EMI source and the EMI victim. These systems use analog (and rarely also digital, e.g., [10] and [11]) circuitry to generate the cancellation signal from a measured quantity in a feedback or feedforward approach. In general, the performance of cancellation systems depends on the matching between EMI and anti-EMI [12]. For AEFs, this matching is systematically limited by…

- finite and frequency-dependent gains of analog amplifiers (i.e. time constants) [8],[9],
- required stabilization elements in the closed loop of feedback AEFs [8],
- deviations in the signal generation of feedforward AEFs [13],
- delay times due to the signal propagation [12], and
- delay times due to the signal processing in digital variants [11],[12].

Considering (quasi-) periodic EMI, the disturbing spectrum consists of discrete and stable harmonics. So, it is feasible to synthesize a broadband cancellation signal from individual sine waves that cancel out the harmonics with the same frequency [12],[14]. By adjusting the amplitudes and phases of the cancelling sine waves, previously limiting effects (like time constants or delay times) can be compensated, and a very high matching between EMI and anti-EMI can be achieved. To maintain the matching and the destructive interference, the artificially synthesized cancellation signal must be synchronized to the EMI. Due to the **s**ynthesized and **s**ynchronized **s**ignals (S³), this method will be referred to as "S³-AEF" in this work.

Until now, S³-AEFs have mostly been applied to the **d**ifferential-**m**ode (DM) EMI of DC-to-DC converters (e.g. [14]-[16]) and inverter systems (e.g. [17],[18]). In many practical systems, there is also **c**ommon-**m**ode (CM) EMI that must be passively attenuated or actively suppressed. In this work, for the first time, an S³-AEF is designed that can simultaneously suppress the DM and CM EMI at the DC input of an inverter system. Due to the two EMI modes, two cancellation signals and two feedback signals are required for the S³-AEF. The design of the S³-AEF and the calculation of the required cancellation signals are no trivial tasks since the injectors can be mutually coupled by the overall system (e.g. [12],[19],[20]). This mutual

coupling can lead to higher power losses if the injectors significantly work against each other. To mitigate this problem, decoupling elements can be integrated (e.g. [12],[19],[20]). The remaining mutual coupling can be respected and mathematically compensated during the synthesis of the cancellation signal (e.g. [12],[19],[20]).

At first, the inverter and the S³-AEF are generally introduced and described. Afterward, the theoretical background for the determination of the ideal cancellation signals is summarized. Then, the S³-AEF is designed and applied to a demonstrator setup. The work is closed by a conclusion and an outlook.

2 Generic description of the application and the S³-AEF

In this section, the considered inverter is presented. For reference to a common EMC standard, it is assumed to be in an automotive application. The occurring CM and DM disturbances are briefly described. Afterward, a generic S³-AEF is inserted to suppress the disturbances on the DC lines.

2.1 Generic inverter system in an exemplary EMC test setup

The considered setup of the inverter system is depicted in Fig. 1. To drive a load (e.g. a motor), the inverter uses three switching half bridges to generate a three-phase system from the DC supply voltage V_{supply}. The switching transistors are the EMI sources of the system. At the **in**put, the motor inverter has a stabilizing capacitance C_{in} that usually consists of large electrolytic and small ceramic capacitors. The inverter considered here is isolated from ground. In reference to the automotive EMC standard CISPR 25 [1], the disturbances on both lines are individually measured against ground by using standardized **a**rtificial **n**etworks (ANs).

The considered inverter generates high-frequency CM and DM EMI, and both modes can be traced back to the switching transistors. The disturbing DM currents flow in opposite directions on the DC supply lines. The disturbing CM currents flow through parasitic capacitances of the switching nodes, load lines and the load itself into ground. They propagate to the ANs, and in the same direction on both supply lines back to the inverter. The CM and DM EMI superpose each other and can be measured as $V_{\text{EMI}}^{@\text{AN,DC}+}(f)$ and $V_{\text{EMI}}^{@\text{AN,DC}-}(f)$ at the measurement ports of the ANs [21].
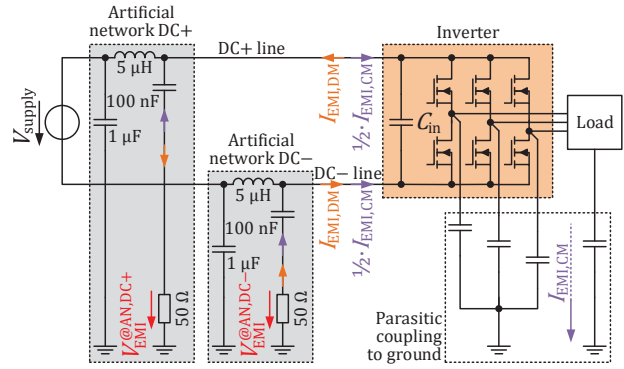
Fig. 1: Inverter system in an automotive EMC test setup according to CISPR 25 [1].
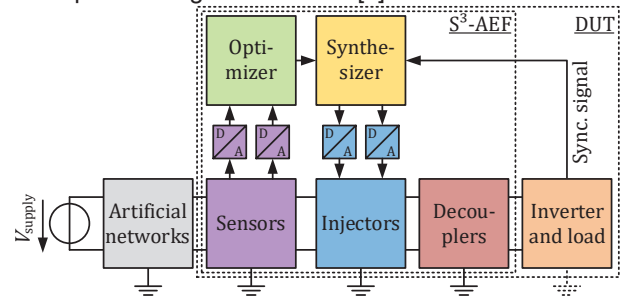
Fig. 2: Block model for the DUT consisting of the inverter system and the S³-AEF.

2.2 Insertion of a generic S³-AEF

In the next step, the inverter system is extended by a digital S³-AEF to form the **d**evice **u**nder **t**est (DUT). A generic block model of the overall system is depicted in Fig. 2.

The high-frequency emissions of the DUT are measured by analog coupling circuits (sensors) that are directly placed at the DC input of the DUT. The sensors pass the high-frequency signals and reject the operating currents and voltages of the inverter system that could otherwise destroy the cancellation hardware. The measured signals are digitized by **a**nalog-to-**d**igital **c**onverters (ADCs) and passed to an optimizer. The optimizer aims at a minimization of the DUT's emissions by adjusting the parameters for the synthesis of the cancellation signals. The cancellation signals are generated from the found parameters by a digital synthesizer, brought into analog domain by **d**igital-to-**a**nalog **c**onverters (DACs) and passed through analog coupling circuits (injectors) into the DC supply lines. The injectors reject the operating currents and voltages of the inverter as well. The necessity of the decoupling circuit will be discussed and explained in Section 3. The synthesizer is synchronized with the inverter by appropriate signals to maintain a destructive interference between EMI and anti-EMI.

3 Determination of the ideal cancellation signals

For the realization of the sensors, injectors and decouplers of the S³-AEF, different topologies can be chosen. It would be possible to use one set of sensor, injector and decoupler for the CM disturbances, and an additional set for the DM disturbances. However, in this work, a single-ended approach is chosen in which the two sets are individually applied to the DC supply lines. It is intended that each injector suppresses the disturbances on its respective line. The resulting topology is depicted in Fig. 3.
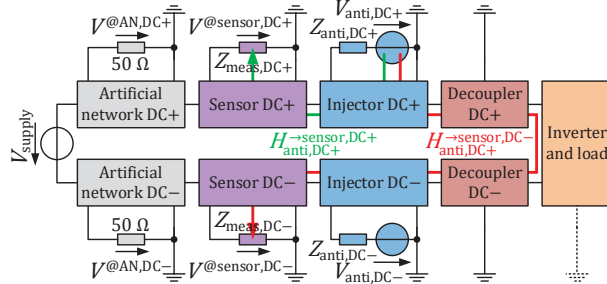
Fig. 3: Topology of a single-ended S³-AEF that separately injects and senses at the DC supply lines (the optimizer, synthesizer, ADCs and DACs are not shown to avoid an overburdened depiction).

In the following, the relevant signals and transfer functions are mathematically described. From this description, the ideal cancellation signals are calculated, and the necessity of decoupling circuits is explained.

3.1 EMI at the sensors

As stated before, the inverter generates CM and DM disturbances that propagate through the overall system and are ultimately emitted from the DUT. The emissions are monitored by the sensors' voltages:

$$\mathbf{V}_{\text{EMI}}^{@\text{sensor}}(f) = \begin{pmatrix} V_{\text{EMI}}^{@\text{sensor,DC+}}(f) \\ V_{\text{EMI}}^{@\text{sensor,DC-}}(f) \end{pmatrix} \quad (1)$$

These are the voltages that must be eliminated to suppress the emissions of the DUT.

3.2 Anti-EMI at the sensors

The cancellation sources of the injectors generate the following cancellation signals (anti-EMI):

$$\mathbf{V}_{\text{anti}}(f) = \begin{pmatrix} V_{\text{anti,DC+}}(f) \\ V_{\text{anti,DC-}}(f) \end{pmatrix} \quad (2)$$

These signals also propagate through the overall system and result in voltage drops over the sensors' measurement ports. Since the two DC supply lines are coupled via the inverter system, both injectors can potentially affect both sensors, and not only the one of the respective lines.

If the system behaves predominantly **l**inear and **t**ime-**i**nvariant (LTI) regarding the high-frequency cancellation signals, the propagation can conveniently be described in frequency domain by using a matrix of complex transfer functions (e.g. [12],[19],[20]):

$$\mathbf{H}_{\text{anti}}^{\rightarrow\text{sensor}} = \begin{bmatrix} H_{\text{anti,DC+}}^{\rightarrow\text{sensor,DC+}} & H_{\text{anti,DC-}}^{\rightarrow\text{sensor,DC+}} \\ H_{\text{anti,DC+}}^{\rightarrow\text{sensor,DC-}} & H_{\text{anti,DC-}}^{\rightarrow\text{sensor,DC-}} \end{bmatrix} \quad (3)$$

The intended coupling (from DC+ to DC+ and from DC− to DC−) can be found on the main diagonal of the matrix. The unintended coupling (from DC+ to DC− and from DC− to DC+) can be found in the remaining matrix entries, i.e. the counter diagonal in the given case. Also note the visualization of the transfer paths in Fig. 3.

Combining Eq. (2) and Eq. (3), the anti-EMI $\mathbf{V}_{\text{anti}}^{@\text{sensor}}$ at the sensors can be described by:

$$\mathbf{V}_{\text{anti}}^{@\text{sensor}}(f) = \mathbf{H}_{\text{anti}}^{\rightarrow\text{sensor}}(f) \cdot \mathbf{V}_{\text{anti}}(f) \quad (4)$$

3.3 Residual EMI at the sensors

The EMI and anti-EMI at the sensors superpose each other and should ideally lead to a destructive interference. Using Eq. (4), The **res**idual EMI $\mathbf{V}_{\text{res}}^{@\text{sensor}}(f)$ can be described by:

$$\mathbf{V}_{\text{res}}^{@\text{sensor}} = \mathbf{V}_{\text{EMI}}^{@\text{sensor}} + \underbrace{\mathbf{H}_{\text{anti}}^{\rightarrow\text{sensor}} \cdot \mathbf{V}_{\text{anti}}}_{\mathbf{V}_{\text{anti}}^{@\text{sensor}}} \quad (5)$$

3.4 Calculation of the ideal anti-EMI

For an ideal cancellation, the residual EMI $\mathbf{V}_{\text{res}}^{@\text{sensor}}(f)$ should equal 0 V. So, the following equation follows from Eq. (5):

$$\Rightarrow \mathbf{0} = \mathbf{V}_{\text{EMI}}^{@\text{sensor}} + \mathbf{H}_{\text{anti}}^{\rightarrow\text{sensor}} \cdot \mathbf{V}_{\text{anti}} \quad (6)$$

To find the ideal anti-EMI, this equation can be rearranged:

$$\Rightarrow \mathbf{V}_{\text{anti}} = -(\mathbf{H}_{\text{anti}}^{\rightarrow\text{sensor}})^{-1} \cdot \mathbf{V}_{\text{EMI}}^{@\text{sensor}} \quad (7)$$

Obviously, $\mathbf{H}_{\text{anti}}^{\rightarrow\text{sensor}}(f)$ must be invertible to do so. So, all injectors must be linearly independent. If the mutual coupling between the injectors is strong, the mathematical solution may become imprecise. A strong mutual coupling will also cause the injectors to work against each other. This may lead to much higher power losses. [12],[19],[20]

Assuming the intended coupling factors are given in the main diagonal of $\mathbf{H}_{\text{anti}}^{\rightarrow\text{sensor}}(f)$ and the unintended ones are represented by the other entries (as assumed in Eq. (3)), it becomes

obvious that the coupling matrix $\mathbf{H}_{\text{anti}}^{\rightarrow\text{sensor}}(f)$ should be diagonally dominant. If the undesired coupling paths through the power electronic system (i.e. the inverter in this case) are too dominant, they can be reduced by adding decoupling elements (e.g. [12],[19],[20]). This will be discussed for a concrete example in the following demonstration.

4 Demonstration

In this section, the S³-AEF is designed and applied to an inverter. At first, the investigated inverter system is introduced, and the goal of the S³-AEF is defined. The digital hardware for the S³-AEF is presented, and the coupling and decoupling circuits are designed. The synthesis of the cancellation signals is described and explained. Last, measurement results are discussed.

4.1 Inverter system and its control

The schematics of the overall test setup are depicted in Fig. 4. The inverter is realized by three GaN half bridges and ceramic and electrolyte capacitors to stabilize the input voltage. It is isolated from ground and has two input lines (DC+ and DC−). The supply voltage is 48 V. The load is made of inductors and resistors, and isolated from ground as well. The transfer power of the inverter is approximately 1 kW. A photograph of the inverter can be found in Fig. 7.

The control signals for the half bridges are calculated by a PC and generated by an **a**rbitrary **w**aveform **g**enerator (AWG) HDAWG8 from Zurich Instruments. These control signals are isolated from ground by digital isolators on the control board of the inverter (note Fig. 7). The switching
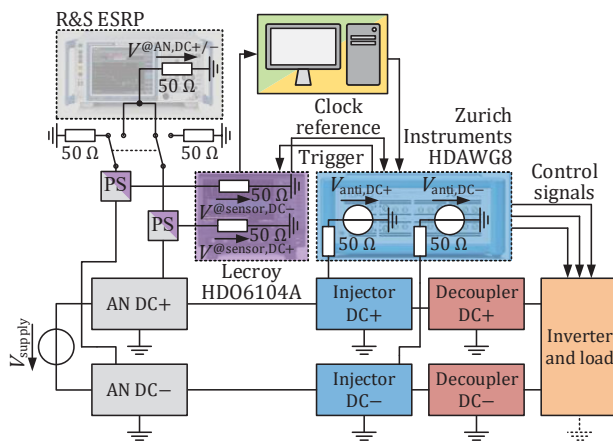
frequency is set to 100 kHz, and the fundamental frequency f_0 of the three-phase system is chosen to 50 Hz. The control pattern is static and repeats itself after each fundamental period of $T_0 = 1/f_0$. Therefore, also the EMI will periodically repeat itself with the fundamental frequency f_0. So, the EMI at the sensors $v_{\text{EMI}}^{@\text{sensor,DC+}}(t)$ and $v_{\text{EMI}}^{@\text{sensor,DC−}}(t)$ can be described by Fourier series (e.g. [21]) with the complex amplitudes $V_{\text{EMI}}^{@\text{sensor,DC+}}(kf_0)$ and $V_{\text{EMI}}^{@\text{sensor,DC−}}(kf_0)$ in a spacing of f_0 [17],[18]. Since the fundamental frequency f_0 equals 50 Hz in this demonstration, the complex amplitudes (that correspond to harmonics) have only a relatively little spacing of 50 Hz.

4.2 Goal of the S³-AEF

The goal of this demonstration is to suppress the EMI measured at the ANs (i.e. $V_{\text{EMI}}^{@\text{AN,DC+}}$ and $V_{\text{EMI}}^{@\text{AN,DC−}}$) in the AM broadcasting range (i.e. 150 kHz-30 MHz, [1]). Considering the fundamental frequency f_0 of 50 Hz, there will be (30 MHz-150 kHz)/50 Hz+1≈600.000 harmonics on each DC supply line that must be actively cancelled out.

The measurement at the ANs is done with an ESRP EMI test receiver from Rohde & Schwarz. The EMI test receiver can only measure one line at a time. The other line will be terminated by a 50 Ω resistor. The EMI test receiver is set up in reference to the automotive standard CISPR 25 [1] with a **r**esolution **b**and**w**idth (RBW) of 9 kHz, a measurement time of 160 ms (multiple periods of the disturbances) and a frequency step of 2.25 kHz. To measure the spectrum in a reasonable time, the FFT-based time domain scan feature is used. The disturbances are evaluated by using the average detector.

4.3 Digital hardware for the prototype S³-AEF

The HDAWG8 is also used to generate the cancellation signals $V_{\text{anti,DC+}}$ and $V_{\text{anti,DC−}}$ (note Fig. 4) to ensure a synchronous operation of the inverter and the S³-AEF. The sampling rate of the device is set to 64 MS/s. According to the Nyquist-Shannon sampling theorem, frequencies of up to 32 MHz can be actively suppressed this way. So, it is well applicable to the considered frequency range of up to 30 MHz.

The sensor signals $V^{@\text{sensor,DC+}}$ and $V^{@\text{sensor,DC−}}$ are acquired by using an oscilloscope HDO6104A from Teledyne LeCroy with a termination impedance of 50 Ω. Oscilloscope and AWG must be synchronized for a simultaneous signal

Fig. 4: Overall test setup with the digital prototype hardware (the sensors, injectors and decouplers will be designed in later steps).

acquisition and generation. For this purpose, the AWG sends a trigger signal to the oscilloscope. To avoid errors due to different clock rates, the AWG uses the reference clock signal of the oscilloscope. In this demonstration, the feedback signal is directly acquired at the ANs. To maintain a termination of 50 Ω for the ANs, 50 Ω **p**ower **s**plitters (PSs) are applied. The PSs attenuate the signals measured by the EMI test receiver by 6 dB. This effect is compensated by adding 6 dB after measurement.

The signal processing is done by a PC with MATLAB. This includes the evaluation of the sensor signals and the optimization and synthesis of the required cancellation signals.

4.4 Design of coupling and decoupling circuits

Last, the analog coupling and decoupling circuits (i.e. injectors and decouplers) must be designed. This requires the consideration of the impedances of the EMI source (i.e. the inverter system) and the EMI victim (i.e. the ANs) as seen from the injectors [12]. For further discussion, Fig. 5 will be considered. Photographs of the realized test setup can be found in Fig. 6 and Fig. 7.

In a first approximation, the inverter and the load can be described by their dominating Y-capacitance against ground (here approximately 900 pF in total) and the stabilizing X-capacitance C_x between DC+ and DC− (here a relatively large value due to the numerous electrolyte and ceramic capacitors in parallel). The ANs may be reduced to the parallel connection of 50 Ω and 5 µH in the considered frequency range (i.e. 150 kHz-30 MHz). The impedance of the 48 V voltage source can be neglected.

The sources of the AWG have a limited voltage range of ±5 V and a source resistance of 50 Ω. To improve the current driving capabilities, two amplifier boards ADA4870ARR-EBZ from Analog Devices are applied. These have an internal resistance of 5 Ω, an amplification factor of 4.5 and a voltage range of ±20 V.

To couple the generated cancellation signals into the system, capacitive injectors have been chosen. Due to safety reasons, the Y-capacitance against ground should be kept small. Since the coupling capacitors act as Y-capacitances, their values are chosen to 6.8 nF.

If there were no decoupling inductors, the two injectors would only be separated by the inverter's stabilizing X-capacitance. Since this capacitance has usually a very small impedance, the injectors
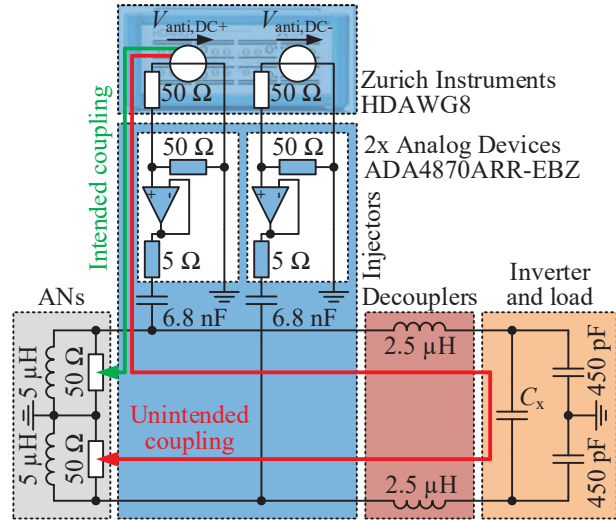
Fig. 5: Schematic of the test setup for the design of the injectors and decouplers.
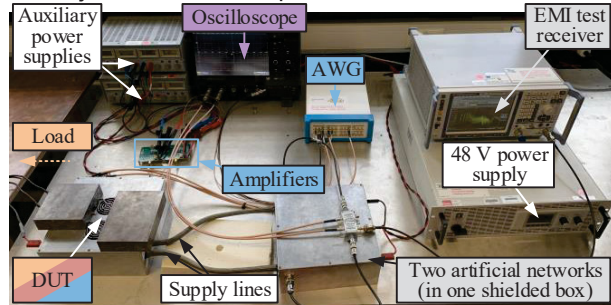
Fig. 6: Photograph of the overall test setup.
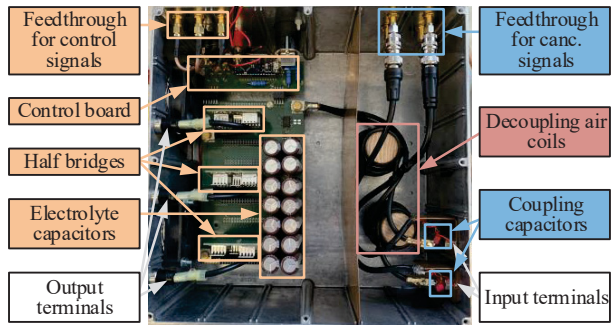
Fig. 7: Photograph of the inside of the DUT's shielding box.

would be strongly coupled with each other. As discussed in Section 3.4, this mutual coupling must be limited. Here, two air coils with 2.5 µH are introduced between the injectors and the inverter. By doing so, the unintended coupling paths are weakened.

4.5 Synthesis of the cancellation signal

As discussed in Section 3, the ideal spectrum for cancellation can be found by Eq. (7). To apply this equation, the EMI spectra at the sensors $\mathbf{V}_{EMI}^{@sensor}$

and the transfer matrix from the injectors to the sensors $\mathbf{H}_{anti}^{\rightarrow sensor}$ must be known. This done by applying the "FFT method" that is described in more detail in [18]. In [12], it is rigorously analyzed.

4.5.1 Identification of the EMI

To find the EMI spectra, the time-domain EMI waveforms $v_{EMI}^{@sensor,DC+}(t)$ and $v_{EMI}^{@sensor,DC-}(t)$ can be measured by using the oscilloscope. Afterward, a **f**ast **F**ourier **t**ransform (FFT) can be applied by the PC to find the complex amplitudes $V_{EMI}^{@sensor,DC}(kf_0)$ and $V_{EMI}^{@sensor,DC}(kf_0)$. For the FFT, the time-domain signal must cover exactly one period or multiple periods of the EMI. Here, the acquired time window must be at least 20 ms long due to the fundamental frequency f_0 of 50 Hz.

4.5.2 Identification of the transfer matrix

The transfer functions from the injectors to the sensors can be found by deactivating the inverter, injecting test signals (for one injector at a time), and evaluating the system's response at the sensors. The test signals can be arbitrarily synthesized from complex amplitudes, but they must cover the relevant frequency range (here 150 kHz to 30 MHz). The system's responses can be analyzed in frequency domain by FFTs. By comparing the spectra of the test signals with the system's responses, the transfer functions can be found. These are depicted in Fig. 8.

As described in Section 3.4, the elements of the main diagonal of the transfer matrix should be dominant. This requirement is fulfilled well for frequencies above approximately 1.5 MHz. Since the coupling capacitors pose only little impedance in this frequency range, the injectors are well coupled to their respective sensors. The transfer functions are even above 0 dB due to the gain of the amplifier boards. Due to the high impedance of the decoupling inductors, the unintended mutual coupling is widely reduced. Between 1 MHz and 1.5 MHz, resonances between the coupling capacitors and the decoupling inductors partially neutralize the decoupling effort. However, due to phase shifts between the transfer functions (not shown here), the inverse of the matrix can still be calculated with sufficient precision. Therefore, suitable cancellation signals can be found. If such phase shifts are not given, the mutual coupling may pose a problem. Between 200 kHz and 1 MHz, the injectors are only partially decoupled. The intended coupling of the injectors to their respective sensors is relatively weak due to the high impedance of the coupling capacitors. The unintended coupling to the respectively other
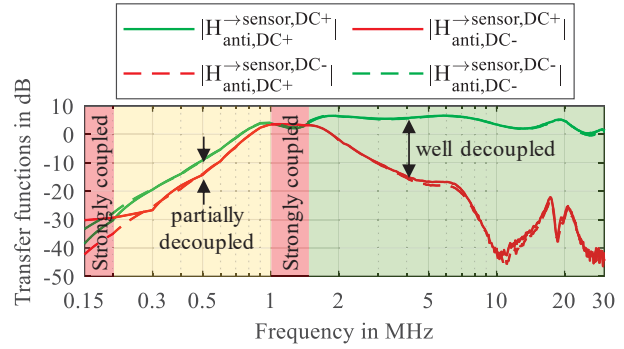
Fig. 8: Identified transfer matrix $\mathbf{H}_{anti}^{\rightarrow sensor}$. The elements of the main diagonal (green curves) should be dominant.

sensors is relatively high since the decoupling inductors pose only little impedance. This effect is the worst below 200 kHz. While it can potentially be a problem, it has been no issue here.

4.5.3 Calculation of the cancellation signals

By using Eq. (7), the complex amplitudes for the cancellation signals $V_{anti,DC+}(kf_0)$ and $V_{anti,DC-}(kf_0)$ can be found. These can be used to synthesize the time-domain cancellation signals $v_{anti,DC+}(t)$ and $v_{anti,DC-}(t)$ by applying, e.g., inverse FFT algorithms. Their fundamental period must equal the one of the disturbances.

It can be expected that the EMI will not be completely cancelled out after one iteration due to, e.g., measurement noise and deviations in the identified transfer functions. To resolve this issue, the algorithm can be applied again to the residual EMI at the sensors. By doing so, the cancellation signals $v_{anti,DC+}(t)$ and $v_{anti,DC-}(t)$ can be successively improved. Here, Eq. (7) is iteratively applied seven times to achieve the best results.

A very brief time window (comprising three switching periods) of the found cancellation signals is depicted in Fig. 9. These signals are generated by the AWG. It can be seen that very complex signals are required to suppress the EMI between 150 kHz and 30 MHz. The signals are inside the available voltage range of ±5 V. If they were not, the amplifier's gain, the coupling and/or the decoupling could be improved.
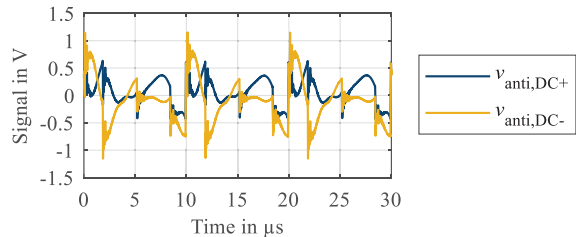
Fig. 9: Short time window of the anti-EMI.

4.6 Measurement results

The measurement results with the EMI test receiver are depicted in Fig. 10 and Fig. 11. Comparing the EMI without S³-AEF and the EMI with **deactivated** S³-AEF, it can be found that the injectors and decouplers introduce some passive attenuation for higher frequencies (comparable to conventional passive filters).

The active EMI suppression achieved by the injected cancellation signals can be found by comparing the EMI with **deactivated** S³-AEF and the EMI with **activated** S³-AEF. The performance of the activated S³-AEF is very high in the complete frequency range. The highest achieved value for the active suppression is 78 dB.

For reference, the class 5 limits of the CISPR 25 are added [1]. The limit lines are fulfilled except for a very narrow frequency range around 1.46 MHz. Since this peak can also be found in the noise floor, it can be assumed to be environmental noise.

The amplifier boards' power consumption for the generation of the cancellation signal can be conservatively estimated. At the input of the amplifiers, half the voltages of $v_{\mathrm{anti,DC+}}(t)$ and $v_{\mathrm{anti,DC-}}(t)$ can be found. These voltages are amplified by the gain of 4.5. In a worst-case scenario, the amplified voltages drop completely over the amplifiers' internal output resistance of 5 Ω. Considering the root-mean-square values of the voltages, the total power of the cancellation signals can be estimated to 43 mW. This value is negligible in comparison to the transfer power of 1 kW.

5 Conclusion and outlook

In this work, an active filter based on synthesized and synchronized signals has been applied for the first time to the common-mode and differential-mode emissions of an inverter system. The fundamental theory has been described, and the cancellation system has been purposefully designed. All important effects, like mutual couplings between injectors, have been discussed and considered in the design. Measurement results in a standard EMC test setup have shown the high potential of the method. The active suppression reaches up to 78 dB in the frequency range from 150 kHz to 30 MHz. The power of the cancellation signals is less than 43 mW and, therefore, negligible in comparison to the transfer power of 1 kW.

Such active cancellation systems may help to reduce the size of passive filter components in
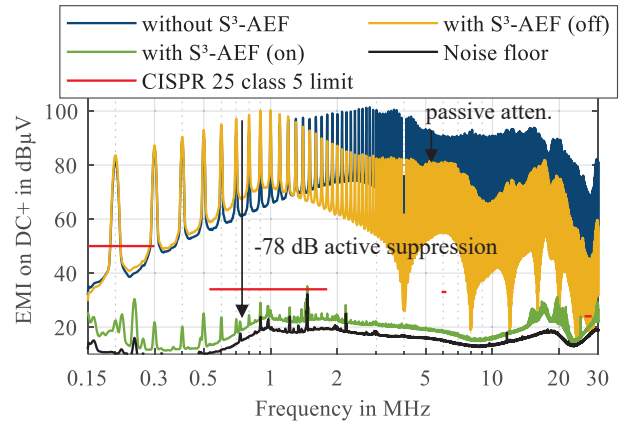
Fig. 10: EMI test receiver measurement at the AN for the line DC+.
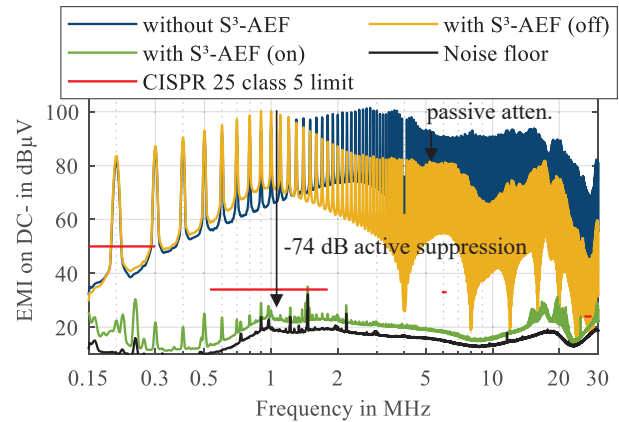
Fig. 11: EMI test receiver measurement at the AN for the line DC−.

practical applications. However, some extensions are required for practical applicability. Here, the optimization has been done for the ANs. In practical applications, there are no ANs and the sensors must be integrated in the device under test. The digital hardware of this demonstrator consists of an arbitrary waveform generator, an oscilloscope and a PC. Obviously, this is no feasible hardware for practical realizations. However, the functionality may be replicated by, e.g., FPGA systems with fast digital-to-analog and analog-to-digital converters. The signal synthesis method used for this demonstration is only applicable to periodic disturbances. While there may be some niche applications that operate periodic, most will be non-periodic. For the non-periodic cases, other implementations (e.g. with predictive approaches) will be required.

6 Acknowledgment

7 References

[1] CISPR 25 – Vehicles, boats and internal combustion engines – Radio disturbance characteristics – Limits and methods of measurement for the protection of on-board receivers, 4th ed., Feb. 2015.

[2] K. Mainali and Ramesh Oruganti, "Conducted EMI mitigation techniques for switch-mode power converters: A Survey," IEEE Trans. Power Electron., vol. 25, no. 9, pp. 2344-2356, Sep. 2010.

[3] P. Lueg, "Process of silencing sound oscillations," U.S. Patent 2 043 416, Jun. 9, 1936.

[4] S. Feng, W. Sander, and T. Wilson, "Small-capacitance nondissipative ripple filters for dc supplies," IEEE Trans. Magn., vol. 6, no. 1, pp. 137-142, Mar. 1970.

[5] J. Walker, "Designing practical and effective active EMI filters," in Proc. Powercon 11 Conf., Dallas, Texas, USA, 10-12 Apr. 1984, Paper I-3.

[6] L. E. LaWhite and M. F. Schlecht, "Active filters for 1-MHz power circuits with strict input/output ripple requirements," IEEE Trans. Power Electron., vol. PE-2, no. 4, pp. 828-290, Oct. 1987.

[7] L. E. LaWhite and M. F. Schlecht, "Design of active ripple filters for power circuits operating in the 1-10 MHz range," IEEE Trans. Power Electron., vol. 3, no. 3, pp. 310-317, Jul. 1988.

[8] N. K. Poon, J. C. P. Liu, C. K. Tse and M. H. Pong, "Techniques for input ripple current cancellation: classification and implementation [in smps]," IEEE Trans. Power Electron., vol. 15, no. 6, pp. 1144-1152, Nov. 2000.

[9] Y.-C. Son and S.-K. Sul, "Generalization of active filters for EMI reduction and harmonics compensation," IEEE Trans. Ind. Appl., vol. 42, no. 2, pp. 545-551, Mar./Apr. 2006.

[10] D. Hamza, M. Pahlevaninezhad and P. K. Jain, "Implementation of a novel digital active EMI technique in a DSP-based dc-dc digital controller used in electric vehicle (EV)," IEEE Trans. Power Electron., vol. 28, no. 7, pp. 3126-3137, Jul. 2013.

[11] J. Ji, W. Chen, X. Yang and J. Lu, "Delay and decoupling analysis of a digital active EMI filter used in arc welding inverter," IEEE Trans. Power Electron, vol. 33, no. 8, pp. 6710-6722, Aug. 2018.

[12] A. Bendicks, "Active Cancellation of Electromagnetic Emissions of Power Electronic Systems by Injecting Synthesized and Synchronized Signals," Ph.D. dissertation, On-board Systems Lab, TU Dortmund University, Dortmund, Germany, 2020. [Online]. Available: https://eldorado.tu-dortmund.de/handle/2003/39212?locale=en.

[13] A. C. Chow and D. J. Perreault, "Design and evaluation of a hybrid passive/active ripple filter with voltage injection," IEEE Trans. Aerosp. Electron. Syst., vol. 39, no. 2, pp. 471–480, Apr. 2003.

[14] A. Bendicks and S. Frei, "Broadband Noise Suppression of Stationary Clocked DC/DC Converters by Injecting Synthesized and Synchronized Cancellation Signals," IEEE Trans. Power Electron., vol. 34, no. 11, pp. 10665-10674, Jan. 2019.

[15] A. Bendicks, T. Dörlemann, S. Frei, N. Hees, and M. Wiegand, "Active EMI Reduction of Stationary Clocked Systems by Adapted Harmonics Cancellation," IEEE Trans. Electromagn. Compat., vol. 61, no. 4, pp. 998-1006, Aug. 2019.

[16] A. Bendicks, T. Osterburg, S. Frei, M. Wiegand, and N. Hees, "Wide-frequency EMI suppression of stationary clocked systems by injecting successively adapted cancellation signals," in Proc. Int. Symp. Electromagn. Compat. Eur., Barcelona, Spain, 2-6 Sep. 2019, pp. 36–41.

[17] A. Bendicks, M. Gerten, and S. Frei, "Aktive Unterdrückung der elektromagnetischen Störungen eines stationär betriebenen Antriebswechselrichters mithilfe von synthetisierten und synchronisierten Gegenstörsignalen," in Proc. Conf. Electromagn. Compat., Cologne, Germany, 12-13 May 2020, pp. 423-432.

[18] A. Bendicks, M. Gerten, and S. Frei, "Active Cancellation of Periodic DM EMI at the Input of a GaN Motor Inverter by Injecting Synthesized and Synchronized Signals," in Proc. Int. Symp. Electromagn. Compat. Eur., Rome, Italy, 23-25 Sep. 2020, accepted for publication.

[19] A. Bendicks, M. Rübartsch, and S. Frei, "Simultaneous EMI suppression of the input and output terminals of a dc/dc converter by injecting multiple synthesized cancellation signals," in Proc. Int. Symp. Electromagn. Compat. Eur., Barcelona, Spain, 2-6 Sep. 2019, pp. 842–847.

[20] A. Bendicks, M. Rübartsch, and S. Frei, "Active cancellation of periodic EMI at all terminals of a DC-to-DC converter by injecting multiple artificially synthesized signals," IEEE Electromagn. Compat. Magazine, Volume 9, Quarter 3, 2020.

[21] C. R. Paul, Introduction to Electromagnetic Compatibility, 2nd ed., Hoboken, NJ, USA: Wiley, 2006.